# Stress Relaxation for Granular Materials near Jamming under Cyclic Compression

Somayeh Farhadi, Alex Z. Zhu, and Robert P. Behringer

Phys. Rev. Lett. **115**, 188001 — Published 29 October 2015

DOI: 10.1103/PhysRevLett.115.188001

# Stress Relaxation For Granular Materials Near Jamming Under Cyclic Compression

Somayeh Farhadi, Alex Z Zhu, and Robert P Behringer
*Department of Physics and Center for Nonlinear and Complex Systems, Box 90305, Duke University, Durham, NC 27708*
(Dated: October 20, 2015)

We have explored isotropically jammed states of semi-2D granular materials through cyclic compression. In each compression cycle, systems of either identical ellipses or bi-disperse disks, transition between jammed and unjammed states. We determine the evolution of the average pressure, $P$, and structure through consecutive jammed states. We observe a transition point, $\phi_m$, above which $P$ persists over many cycles; below $\phi_m$, $P$ relaxes slowly. The relaxation time scale associated with $P$ increases with packing fraction, while the relaxation time scale for collective particle motion remains constant. The collective motion of the ellipses is hindered compared to disks, due to the rotational constraints on elliptical particles.

*Introduction:* Particle systems near jamming exhibit several signature features, including dynamical slowing down, and heterogeneous dynamics[1, 2]. Systems of interest include colloids, molecular glass formers, and granular materials[3–6]. Although all these systems can jam, granular materials, which we consider here, have the experimental advantage of accessibility at the particle scale. We use this feature to explore the dynamics of isotropically driven disordered materials near jamming.

Although these systems all share the certain common features, several aspects distinguish studies of them, including excitation mechanisms, and interparticle interactions. In molecular and colloidal systems, temperature provides homogeneous driving. In granular systems, temperature is an irrelevant variable, and driving must be provided externally. In past granular studies, driving came from vibration or tapping[7–9], by biaxial strain[10], or by shear[11–14]. Much of the work on vibration and tapping has been summarized in Richard et al.[7], and usually involve energy input on rapid time scales and in ways that may not be isotropic and uniform. Alonso-Maroquín and Herrmann[10] focused on the role of friction at contacts for biaxial cyclic strain applied to systems of irregular 2D polygons which always existed in a jammed state (with nonzero stresses). Shear strain can be applied on any time scale, but it is anisotropic, and not necessarily homogeneous; e.g., shear failures are often localized[15, 16]. The first point of the present experiments is to understand the effect of jamming on granular systems when the driving mechanism is (relatively) uniform, isotropic and on slow time scales.

Previous studies of spatio-temporal granular dynamics near jamming have typically involved spherically symmetric particles: disks in 2D, spheres in 3D. In recent experiments, we showed that tangential forces for frictional particles significantly change stable states near jamming[17], and help stabilize the granular network ('force chains'). If friction stabilize granular networks by limiting rotation, it is natural to probe the possibly similar role played by geometry, and this is the second question that we address here. As we show below, although both types of systems slow down under cyclic driving as the density grows, the characteristic time scales for ellipses is significantly greater than for disks.

In the present experiments, we cyclically and isotropically compress/expand our granular systems by small amounts, starting from a packing fraction $\phi$, just below isotropic jamming, and compressing to a $\phi$ that is above isotropic jamming. We measure the mean pressure, $P$, and the collective dynamics in the most compressed states for very large numbers of cycles. Under this protocol, the system may slowly find more compact configurations. The time associated with this evolution becomes large as $\phi$ for the compressed state grows, whereas the time scale for the evolution of inhomogeneities of particle motion remains roughly constant. We emphasize that the most compressed $\phi$ during a cycle is always above isotropic jamming, e.g. $\phi_c \simeq 0.84$ for disks [18] and $\phi_c \simeq 0.91$ for ellipses[19].

*Experiment:* The experiments consisted of cyclic isotropic compression of quasi-2D systems of bidisperse disks and systems of identical ellipses with aspect ratio $\sim 2$. A schematic of the setup is shown in Fig. 1. The particles were confined in a square container, a biax, where two of the confining walls were stationary, while the other two were displaced using linear motors. The distance between opposing pairs of walls has a spatial resolution of $\sim 10^{-6}$m. The number of particles was kept constant at 2400 in all the experiments. By changing the confining area of the biax [17], we changed the packing fraction. The packing fractions, $\phi$, of the fully compressed states were chosen above the isotropic jamming point (point J). Here we refer to point J, as the packing fraction of a system under isotropic compression, where the coordination number, Z, begins to grow as a power law [19]. We have introduced point J in this study, because any cyclic dynamics died out very quickly if the system is below and far from isotropic jamming point. The particles were photoelastic, which allowed us to measure the local pressure acting on each particle. Before starting any compression cycle, the system was prepared in a stress-free state. It was then quasi-statically

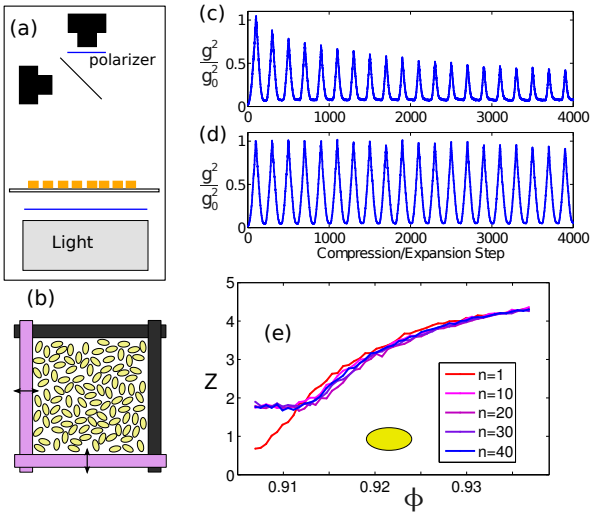


FIG. 1. Schematics of the biax. a) Particles are confined inside a square region. b) Side view. c,d) Time series of global $g^2$ for two sets of cyclic compression of ellipses performed in different packing fraction intervals of c) [0.868, 0.896], and d) [0.906, 0.937]. The values of $g^2$ are normalized by $g^2$ at the most compressed state of the first cycle ($g_0^2$). The system is compressed by %1.6 in a series of much smaller quasi-static steps. e) Coordination number, $Z$, vs. packing fraction. All the particles (including rattlers) are counted in calculating $Z$. The power law growth of $Z$ at $\phi \simeq 0.91$ indicates the onset of isotropic jamming transition. Here, $n$ is the compression cycle. $n = 1$ corresponds to the transient response.

compressed via many small strain steps (about 0.016%) for a typical total volumetric strain of 3.2%. Next, it was quasi-statically expanded to its initial strain-free state. This process was repeated for multiple cycles. Some initial runs were made for which the system was imaged at every strain step for multiple compression steps and relaxations. For longer numbers of compression cycles (up to $\sim 1000$ cycles), the system was strained as above, but imaged only once at the maximum compressive strain for each cycle. Before imaging at this strain extremum, the system was allowed to relax. The imaging was carried out using two synchronized digital cameras, one of which recorded a polarized image which yielded the photoelastic response of the system, while the other recorded a normal (unpolarized) image. These two images enabled us to measure the local stress on each particle, and to track the particles, including their centers, and orientations (for ellipses).

The quasi-2D particles, either circular (disks) or ellipses, are machined from sheets of Vishay polymer PSM-4 that are 0.635 cm thick. The semi-minor axis of the ellipses is $b \simeq 0.25$ cm, and the aspect ratio is 1.85. The system of disks is bi-disperse, where the ratio of small-to-large particles is kept at about $4.5 : 1$. The radius of small disks is $r_s \simeq 0.38$ cm, and the radius of larger particles is $r_l \simeq 0.44$ cm. The particles rest on a horizontal Plexiglas sheet (Fig. 1a) that has been lubricated by a layer of fine powder. As shown in Fig. 1a, a circularly polarized beam passes through the Plexiglas sheet and the particles from below, and then through a beam splitter placed over the setup. The beam splitter provides two identical images, one of which is viewed without a polarizer by the horizontal camera, while the other, passes through a crossed circular polarizer (with respect to the bottom polarizer) and is viewed by the top camera. The two cameras acquire images simultaneously. As a result, one camera records the photoelastic response of the system (polarized image), and the other camera yields a direct image (normal image) of the particles for tracking. We extracted the local stress acting on each particle, which is encoded in the photoelastic response, using an established empirical measure which we call $g^2$. This quantity is the gradient squared of the transmitted photoelastic image intensity integrated over the pixels associated with each particle[12]. Before computing $g^2$, we first filter the photoelastic images, leaving only the green channel of the original color image, which corresponds to the optimum color response of the polarizers. The global stress is found by averaging $g^2$ over all particles in each image at a given strain.

*Global stress response:* Fig. 1(c,d) show time series of the global stress of the ellipses for two packing fraction intervals (i.e. minimum and maximum $\phi$'s), which are obtained by incrementally compressing/expanding the system over a number of cycles. In Fig. 1(c,d), the global values of $g^2$ are normalized by the global $g^2$ at the most compressed state of the first cycle ($g_0^2$), which always corresponds to a density that is above the isotropic jamming point. For the lower packing fraction, Fig. 1c, we see a gradual drop of the maximum global $g^2$. Although the system is effectively "jammed" for part of each cycle, after enough cycles, the stress relaxes to a measurably lower value. We then track the evolution of these jammed states by considering $g^2$ for the most compressed states. The corresponding time series of $g^2/g_0^2$, for several packing fractions of ellipses and disks (the most compressed $\phi$ is used as a label here), are shown in Fig. 3a. Here, we emphasize the relaxation which occurs for states with the most compressed packing fractions that are above the isotropic jamming point. However, there is a largest $\phi_m$ such that we do not see significant particle or stress relaxation over $\sim 1000$ cycles. For instance, the time series of disks corresponding to $\phi = 0.868$ in Fig. 3a pertains to a packing fraction which is lower than $\phi_m^{disks}$, even though the fully compressed density for this data is above the isotropic jamming density of $\phi \simeq 0.84$. At a higher packing fraction (i.e. $\phi = 0.883$), the global $g^2$ is persistent for many cycles, in the sense that there is no overall change in the peak $g^2$ with cycle number. We conclude that there is a range of $\phi$ for which the very small amount of spatial freedom, coupled with the compressive/dilational driving is sufficient to allow structural

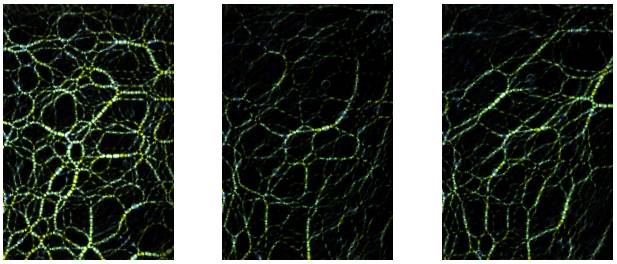

FIG. 2. Photoelastic images showing how the force network evolves over 999 cycles of cyclic compression, applied to a system of disks at $\phi = 0.863$. The cycle number of images from left to right are: 1, 500, and 999.

rearrangement.

In Fig. 2, we show photoelastic images of disks for the maximum compressions of cycle 1, 500 and 999. Note that the stress network of the most compressed states changes spatially while the overall stress relaxes over cycle number.

In order to quantify the long term stress relaxation as in Fig. 3a, we fit the time series to the functional form $\frac{g^2}{g_0^2} = A(\frac{t_0}{t}+1)^a$, which captures both the initial relatively fast drop and the long-time saturation to a final value, $g_\infty^2/g_0^2$. Since, we have one more constraint on parameters at $t = 1$, i.e. $A(t_0+1)^a = 1$, the functional form reduces to $\frac{g^2}{g_0^2} = (\frac{t+t_0}{t(t_0+1)})^a$. The fitted curves are shown by solid lines in Fig. 3a. The large time value is $g_\infty^2/g_0^2 = (1+t_0)^{-a}$, and it is straight forward to compute the time $t_{1/2}$ for $\frac{g^2}{g_0^2}$ to fall from 1.0 to $(1+g_\infty^2/g_0^2)/2$.

From the parameters $a$ and $t_0$, obtained from the least squares fits, we find $g_\infty^2/g_0^2$ and $t_{1/2}$ as a function of density for both disks and ellipses, which we then show in Fig. 3b,c. Although there is a fair bit of scatter, the time scale $t_{1/2}$ grows strongly and $g_\infty^2/g_0^2$ jumps quickly to 1.0, above a characteristic maximal packing fraction, $\phi_m$, where the system becomes effectively frozen; at least on the time of these experiments, there is little evolution of the global stress for either ellipses or disks for cyclic compression carried out above this density. From $g_\infty^2/g_0^2$ values, we estimate $\phi_m \simeq 0.88$ for disks, and $\phi_m \simeq 0.93$ for ellipses. For densities above $\phi_m$, the system maintains a global $g^2$ and a memory of its previous state for seemingly arbitrarily large numbers of compression cycles. To the best of our knowledge, this work is the first observation of such an effect.

*Particle motion vs. stress evolution:* Given that the present systems can compact over long time scales, an interesting question is whether the dynamical process of gradual compaction is associated with identifiable, and possibly heterogeneous, structural changes (i.e. in the particle positions). In order to probe the effect of particle motion, we first consider the mobility of particles, defined as the displacement of the particle for a given time

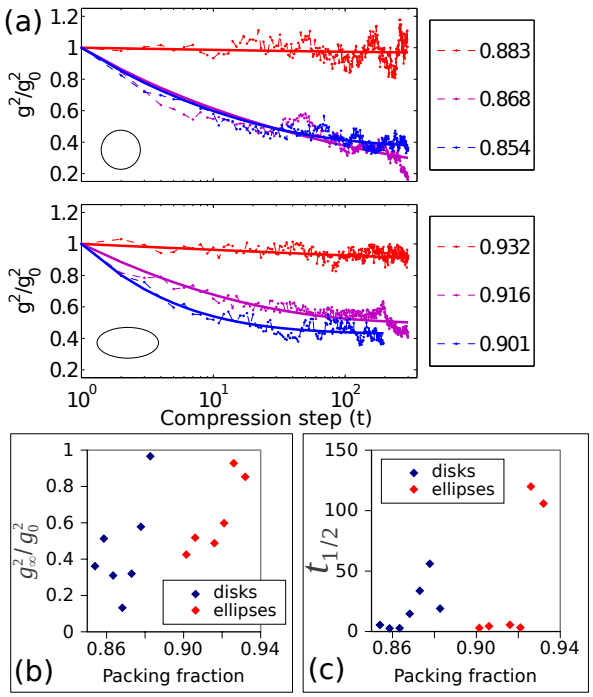


FIG. 3. a) Time series of global $g^2$ for representative systems of disks, and ellipses under maximum compression. Colors represent packing fractions at the most compressed state of each cycle. b) Data for $g_\infty^2$, determined from fit to $g^2/g_0^2 = (\frac{t+t_0}{t(t_0+1)})^a$. c) Relaxation time for $\frac{g^2}{g_0^2}$ to relax halfway between its initial value of 1, and $g_\infty$.

delay, $\tau$, relative to the mean displacement of all particles (Here, time represents the number of compression cycles). Fig. 4 shows data for two different time delays, $\tau = 10$, and $\tau = 1000$ in a compression experiment on ellipses. Particles with similar mobility are represented by similar colors in Fig. 4. Specifically, the colors correspond to the following fractional changes relative to all the particles: red: $0.90 \pm 0.1$; green: $0.70 \pm 0.10$; blue: $0.50 \pm 0.10$; and black: $0.20 \pm 0.20$. Although the spatial distribution of most mobile particles change substantially over time, the regions of comparable mobility form very large clusters. This indicates heterogeneous dynamics both in time and space. The dense structure of these clusters suggests that there are at best small local rearrangements of the particles.

As an alternative approach of quantifying this heterogeneous dynamics, we have studied the 4-point susceptibility, $\chi_4(\tau)$, which indicates the extent of temporal correlation of dynamics at any pair of spatial points[3]. $\chi_4(\tau)$ is defined as: $\chi_4(\tau) = N[< Q_s(\tau)^2 > - < Q_s(\tau) >^2]$. We choose $Q_s(t) = \frac{1}{N}\sum_{i=1}^{N} w(|r_i(t) - r_i(0)|)$, with

$$w = \begin{cases} 1 & \text{if } |r_i(t) - r_i(0)| < l, \\ 0 & \text{otherwise} \end{cases}$$

$N$ is the number of particles, $r_i(t)$ indicates the particle

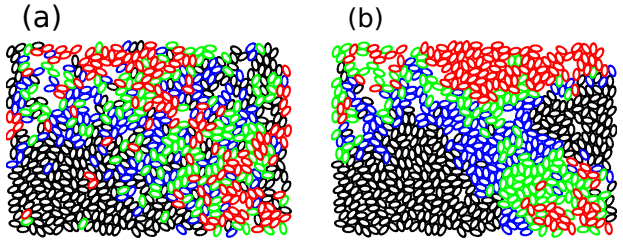


FIG. 4. Mobility of the particles (ellipses) in an arbitrary time. The packing fraction of the system is $\phi = 0.932$. The time delay, $\tau$, equals to a) 10 cycles, and b) 1000 cycles. The various colors represent particles with similar mobility range. Specifically, the colors correspond to the following fractional changes relative to all the particles: red: $0.90 \pm 0.1$; green: $0.70 \pm 0.10$; blue: $0.50 \pm 0.10$; and black: $0.20 \pm 0.20$.

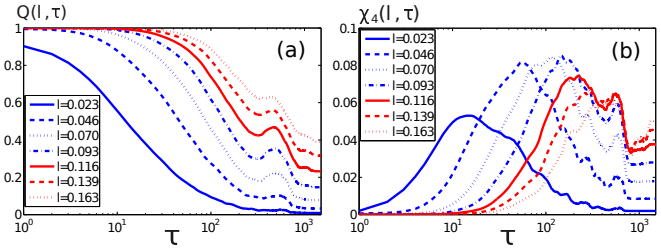


FIG. 5. $Q_s(\tau)$ and $\chi_4(\tau)$ for a system of isotropically compressed ellipses with (highest) packing fraction of $\phi = 0.916$. The unit of length scale, $l$, is the semi-minor axis of an ellipse.

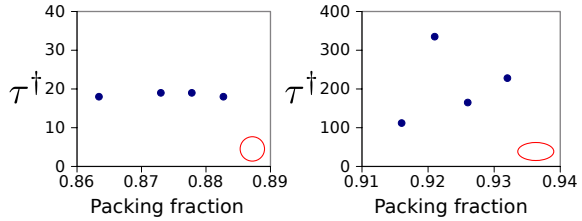


FIG. 6. $\tau^\dagger$ vs. packing fraction, $\phi$, for systems of ellipses and disks. As seen, the average value of $\tau^\dagger$ is about an order of magnitude larger for ellipses compared to disks.

positions at time $t$, for a length scale $l$. The averages are taken over all the particles and over all starting times. $Q_s(\tau)$, which is referred to as the *self overlap order parameter*, is a measure of particle mobility, and is quantified by a length scale $l$[3]. We plot $Q_s(\tau)$ and $\chi_4(\tau)$ vs. $l$, in Fig. 5. As seen, $Q_s$ varies from 1 to 0 as the time delay $\tau$ increases. On the other hand, $\chi_4$ has a maximal point for each $l$, which basically characterizes a time delay, $\tau^*$, by which the particles on average move more than the length scale $l$.

As seen in Fig. 5b, $\chi_4$ is maximal for the characteristic length scale $l^\dagger \simeq 0.093$. We now take the characteristic $l^\dagger$ for each packing fraction, and find the corresponding maximal $\tau^\dagger$. The data are demonstrated in Fig. 6. We note that similar structure for $\chi_4$ has been obtained under much more energetic driving conditions by Dauchot and coworkers[4]. There are several remarkable features in these data. First, the typical length scales for $l$ are only a fraction of a particle diameter; the particles are largely confined. Second, the characteristic times $\tau^\dagger$ are relatively insensitive to $\phi$, but are an order of magnitude greater for ellipses than for disks.

These results beg the question, where should one look to observe the stress relaxation demonstrated in Fig. 3a. In fact, the distribution of forces demonstrated by photoelastic response in Fig. 2, shows that although the particles may move very little, even a tiny bit of freedom allows the force network to evolve and relax substantially in time.

*Conclusions:* We have observed transient stress states that occur for both systems of disks and ellipses that are cyclically compressed by a modest amount above the isotropic jamming point (point $J$). The global stress relaxes to a stationary value in the course of many compression cycles. The time corresponding to stress relaxation grow substantially above a characteristic packing fraction, $\phi_m$ (ellipses: $\phi_m = 0.93$; disks: $\phi_m = 0.88$). We have sought to identify the origin of the stress relaxation. To do so, we first characterized the structural changes by computing relative mobilities and, $\chi_4$. In particular, the characteristic time scale, $\tau^\dagger$, varied rather little with $\phi$ whereas the stress relaxation showed a significant change by increasing $\phi$. However, the analysis of $\chi_4$ did identify significantly longer times for $\tau^\dagger$ in the case of ellipses, which we attribute to the fact that ellipses are substantially confined by their inability to rotate. In fact, the most clearly identifiable relaxation occurs in the force network, even though there is minimal particle motion. An interesting issue for future work concerns the extent to which inter-particle friction plays a role in the relaxation process. For disks, friction may be more important in stabilizing packings than for ellipses, where rotational constraints do occur even without friction.

This work is supported by NSF grant DMR-1206351, NASA Grant NNX10AU01G, and ARO grant W911-NF-1-11-0110.

[1] L. Berthier, G. Biroli, J. Bouchaud, L. Cipelletti, W. van Saarloos, *Dynamical Heterogeneities in Glasses, Colloids, and Granular Media*, Oxford University Press (2011).
[2] N. Lačević, SC. Glotzer, J. Phys. Chem. B **108**, 19623-19633 (2004).
[3] AS Keys, AR Abate, S. Glotzer, D. Durian, Nature Phys. **3**, 260-264 (2011).
[4] O. Dauchot, G. Marty, G. Biroli, PRL **95**, 265701 (2005).
[5] S. Glotzer, J Non-Cryst. Solids **274**, 342-355 (2000).
[6] C. Coulais, R. P. Behringer and O. Dauchot, EPL **100**, 44005 (2012).
[7] P. Richard, M. Nicodemi, R. Delannay, P. Ribière, D.

Bideau, Nature Mater. **4**, 121-128 (2005).
[8] P. Philippe, D. Bideau, EPL **60**, 677 (2002).
[9] F. Lechenault, O. Dauchot, G. Biroli, J. P. Bouchaud, EPL **83**, 46003 (2008).
[10] F. Alonso-Marroquín and H. J. Herrmann, Phys. Rev. Lett. **92**, 054301 (2004).
[11] S. Farhadi and R. P. Behringer, PRL **112**, 148301 (2014).
[12] D. Howell, R. P. Behringer, C. Veje, PRL **82**, 5241-5244 (1999).
[13] J. H. Snoeijer, W. G. Ellenbroek, T. J. H. Vlugt, and M. van Hecke, Phys. Rev. Lett. **96**, 098001 (2006).
[14] J. Ren, J. A. Dijksman and R. P. Behringer, Phys. Rev. Lett. **110**, 018302 (2013).
[15] H. M. Jaeger, S. R. Nagel, Science **255**, 1523 (1992).
[16] H. M. Jaeger, S. R. Nagel, R. P. Behringer, Rev. Mod. Phys. **68**, 1259 (1996).
[17] T.S. Majmudar and R. P. Behringer, Nature **435**, 1079 (2005).
[18] T.S. Majmudar, M. Sperl, S. Luding, and R.P. Behringer, Phys. Rev. Lett. **98**, 058001 (2007).
[19] Shape Effects on Jamming of Granular Materials, Chapter 6, Ph.D. Thesis, Duke University, 2012 (unpublished).